Proposal for a pulsed laser system for Compton polarimetry at the future EIC facility

Ciprian Gal[1,2], Dave Gaskell[3], Kent Paschke[4], Shukui Zhang[3], Abhay Deshpande[1,2]
[1]Stony Brook University, [2]Center for Frontiers in Nuclear Science,
[3]Jefferson Lab, [4]University of Virginia

June 2020

Abstract

The Electron Ion Collider will provide some of the highest luminosities ever achieved at in a collider. This will allow for unprecedented access to high precision multi dimensional measurements of the structure of the fundamental building blocks of matter. To make effective use of this data all systematic sources of uncertainty need to be well under control. This proposal addresses one of these sources, namely the precision measurement of the electron beam polarization.

Contents

1 Motivation

The high precision studies of the longitudinal spin of the proton (g_1 structure function) or electroweak structure functions will require very tight control of all sources of systematic uncertainty (potentially to below 1%). To achieve the precision required by some of these measurements a constant monitoring of each individual colliding electron bunch over their lifetime is required. To achieve this we rely on the Compton scattering process. Compton polarimetry has a long history of use at both collider and fixed target facilities because it can provide a non-destructive measurement. It has also been the standard technique used in storage rings (such as HERA [6]). Recently, high precision results have been obtained in Hall C at Jefferson Lab [1] with lower than 1% systematic uncertainty.

We plan to make use of the lessons from previous polarimeters and adapt them to the EIC environment.

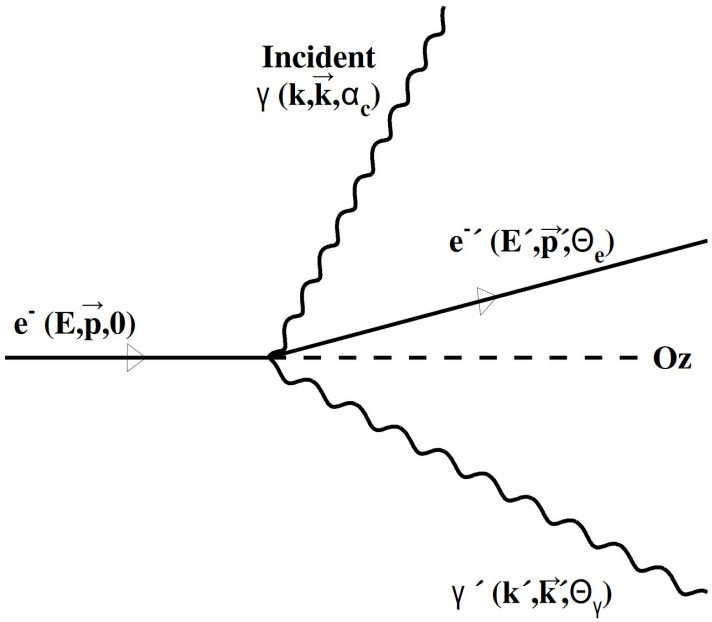

Figure 1: Compton scattering kinematics [3].

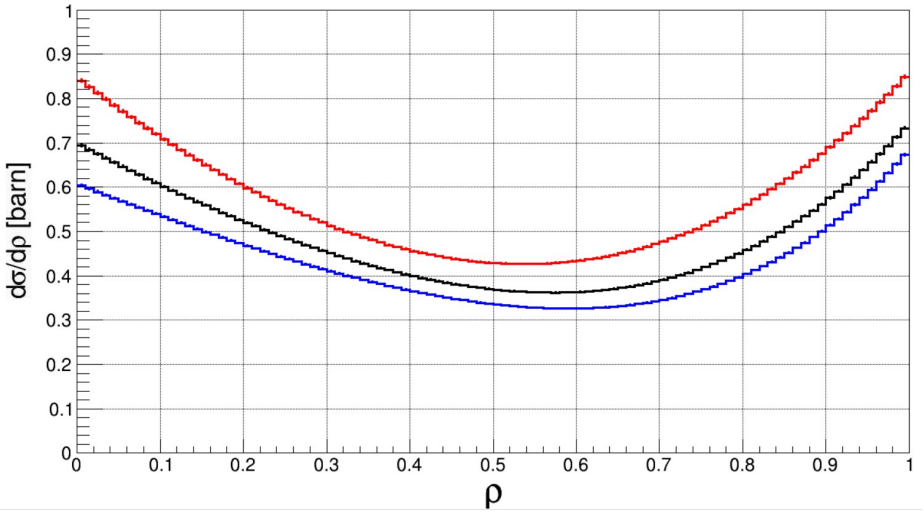

Figure 2: Compton unpolarized cross-section as a function of back-scattered photon energy, for electron energy 5, 12 and 18 GeV (red, black and blue respectively) and laser wavelength of 532 nm.

The kinematics for Compton scattering can be seen in figure 1. An important feature of the detailed derivation presented in [3] is the non-zero crossing angle (α_C) between the incoming photon and the electron direction. While

it complicates the derivation, it is important because in practice we cannot have a laser system on the same axis as the electron beam.

The scattering process is described in detail in several papers (see [3] or references in [2]). In the following we make use of the formalism presented in [2]. The unpolarized cross section is given by equation 1 and can be seen in figure 2 as a function of the fractional photon energy for three possible energies of the electron beam.

$$\frac{\mathrm{d}\sigma}{\mathrm{d}\rho} = 2\pi r_0^2 a \left[\frac{\rho^2(1-a)^2}{1-\rho(1-a)} + 1 + \left(\frac{1-\rho(1+a)}{1-\rho(1-a)} \right)^2 \right] \tag{1}$$

In equation 1:

- r_0 is the classical electron radius 2.819 10^{-13} cm,
- $\rho = k'/k'_{max}$ is the scattered photon energy normalized to the maximum energy,
- and the kinematical factor $a = \left(1 + 4kE_{\mathrm{laser}}/m^2\right)^{-1}$.

The longitudinal and transverse asymmetries are given by equations 2 and 3 below:

$$A_{long} = \frac{2\pi r_0^2 a}{\mathrm{d}\sigma/\mathrm{d}\rho}(1-\rho(1+a)) \left[1 - \frac{1}{(1-\rho(1-a))^2} \right] \tag{2}$$

$$A_{trans} = \frac{2\pi r_0^2 a}{\mathrm{d}\sigma/\mathrm{d}\rho} \cos(\phi) \left[\rho(1-a) \frac{\sqrt{4a\rho(1-\rho)}}{(1-\rho(1-a))} \right] \tag{3}$$

Figure 2 shows the longitudinal asymmetry as a function of the fractional photon energy. One important feature of the asymmetry is the change in sign that occurs between 0.5 and 0.65 of the maximal photon energy. This zero-crossing allows for a simple calibration of the measurement. As can be seen the peak asymmetry increases with electron beam energy reaching almost 46% for 18 GeV. Due to the dependence on energy, rather than spacial positioning this measurement method lends itself easily to a multiple particle measurement method which can substantially reduce the measurement time needed to reach a high level of precision.

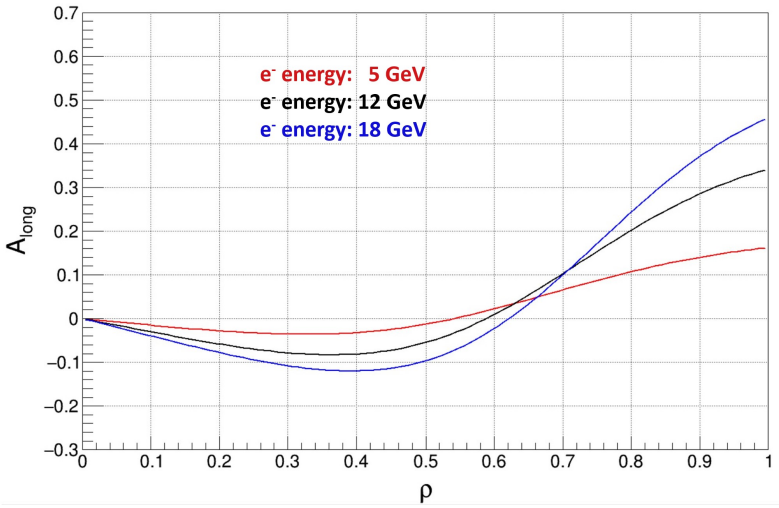

Figure 3: Longitudinal asymmetry as a function of back-scattered photon energy, for electron beam energies of 5, 12 and 18 GeV (red, black and blue respectively) and a 532 nm laser system.

Figure 4 shows the photon transverse asymmetry as a function of vertical position 25 meters away from the interaction point. Similarly to the longitudinal asymmetry the asymmetry for the 18 GeV interaction produces a large analyzing power. However, this analyzing power is much closer to the horizontal central line of the detector making detection harder.

A more general way to describe the transverse asymmetry is to plot it as a function of azimuthal scattering angle. Figure 5(13) shows the transverse asymmetry (on the z-axis) as a function of the fractional photon energy (on the x axis) and azimuthal scattering angle (on the y axis). This asymmetry is generally extracted through an UP-DOWN spatial asymmetry and is maximized at about 70% of the maximum photon energy. As can be seen from figure 4 the vertical distance in a typical measurement environment are fairly small between the maximum and minimum of the asymmetry distribution. This makes multiple particle (integrating) measurements very challenging.

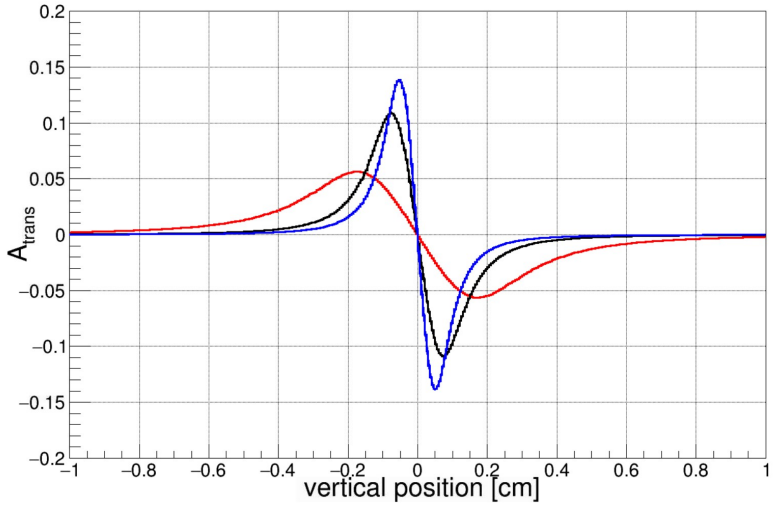

Figure 4: Transverse asymmetry as a function of vertical position 25 m away from the interaction point, for electron beam energies of 5, 12 and 18 GeV (red, black and blue respectively) and a 532 nm laser system.

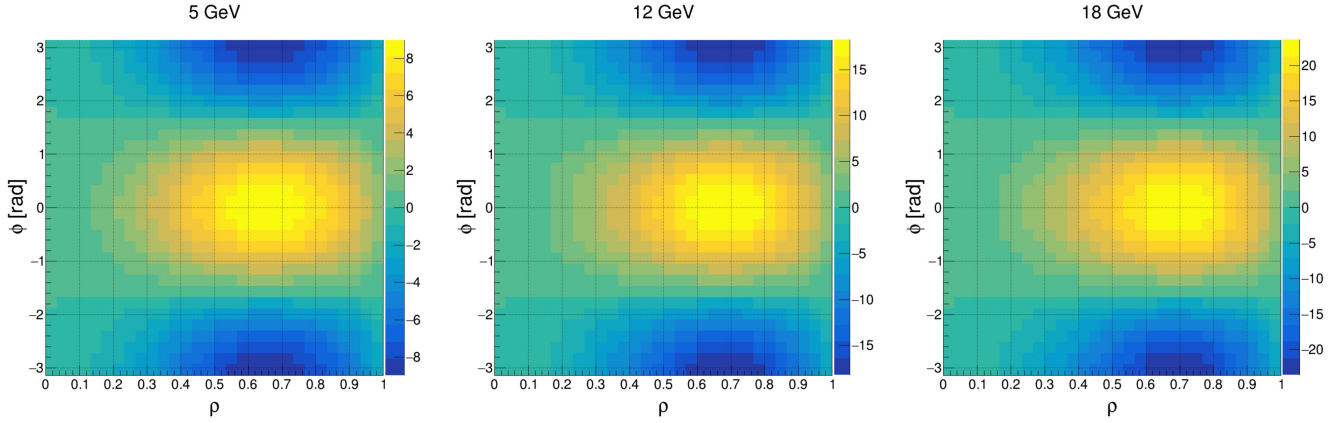

Figure 5: Compton transverse asymmetry (z-axis) as a function of back-scattered photon energy and azimuthal scattering angle.

1.1 EIC Transverse polarimeter at IP12

Due to the accelerator design the main electron polarimeter will be located in the EIC ring at the 12 o'clock locations (IP12), where the polarization of the electron bunches will be vertical. This constrains the measurement type to be a differential measurement (need the capability to measure each individual scattered particle). While this method is significantly slower than the integration method it does put less constraints on the laser system (specifically the total power needed). Table 1 shows the basic electron beam parameters at IP12 for 3 considered running energies. Important to note are the large transverse sizes of electron beam at the interaction region and the different frequencies for the bunches at the IP.

beam property	5 GeV	10 GeV	18 GeV
Bunch frequency	99 MHz	99 MHz	24.75 MHz
Beam size (x)	390 μm	470 μm	434 μm
Beam size (y)	390 μm	250 μm	332 μm
Pulse width (RMS)	63.3 ps	63.3 ps	30 ps
Intensity (avg.)	2.5 A	2.5 A	0.227 A
Bunch lifetime	>30 min	>30 min	6 min

Table 1: Beam parameters at IP12 for three different possible beam energies.

Figure 6(14) shows the distribution of the back-scattered photons and scattered electrons 25 meters away from

the IP. The particles were passed through a realistic first pass implementation of the magnetic configuration at the IP12 (which can be see in the horizontal separation of the scattered electrons). For the electrons note the large diference between the vertical and horizontal scales.

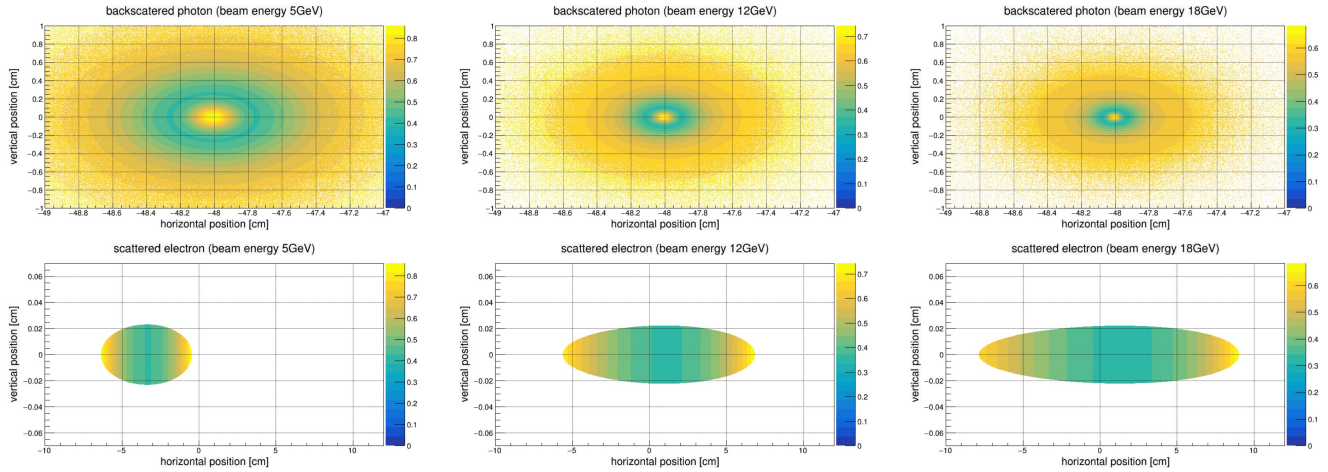

Figure 6: Compton unpolarized cross-sections (on the z axis) as a function of transverse position for 3 different beam energies.

Figure 7(15) shows the analyzing powers (on the z axis) 25 meters away from the IP. As noted from the vertical 1D plots (see figure 4) the larger analyzing powers sit spatially closer together while being significantly larger at higher energies.

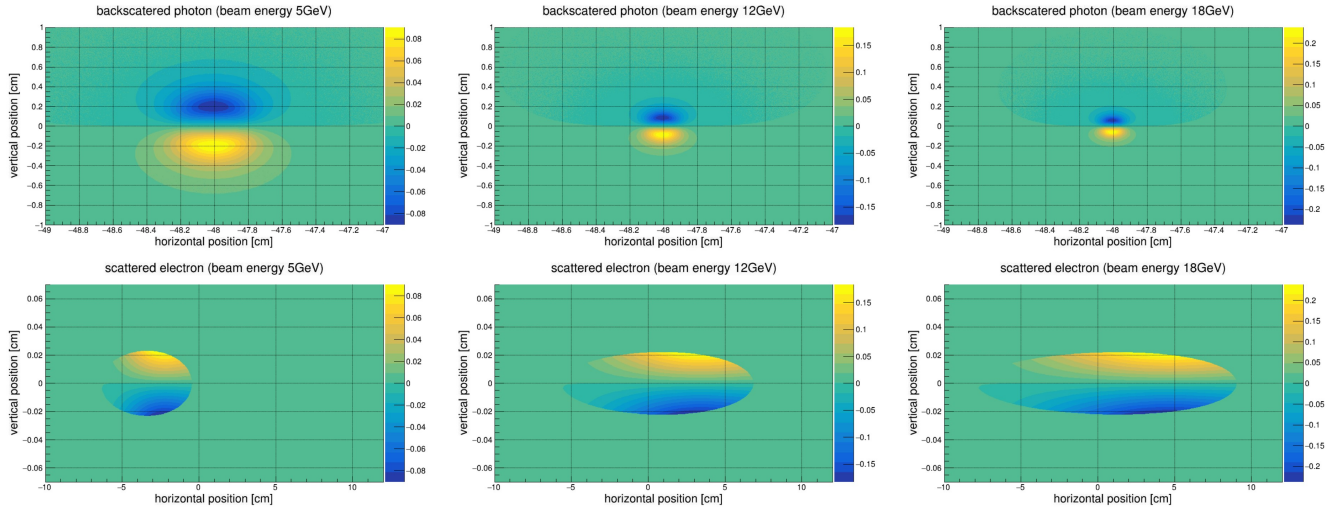

Figure 7: Compton analyzing powers (on the z axis) as a function of transverse position for 3 different beam energies.

Using the average analyzing power over the detector face one can calculate the time needed to reach a certain level of precision. As detailed in [3] this time is inversely proportional to the square of the raw asymmetry (which changes with measurement method):

$$t_{meth} = \left(\mathcal{L}\ \sigma_{\text{Compton}}\ \mathrm{P_e^2 P_\gamma^2}\ \left(\frac{\Delta \mathrm{P_e}}{\mathrm{P_e}} \right)^2\ \mathrm{A_{meth}^2} \right)^{-1} \tag{4}$$

The $\mathrm{A_{meth}^2}$ for the integrated, energy weighted integrated, and differential methods can be written as a function analyzing power and ordered as follows:

$$\langle \mathrm{A} \rangle^2 < \frac{\langle \mathrm{E} \cdot \mathrm{A} \rangle^2}{\langle \mathrm{E}^2 \rangle} < \langle \mathrm{A}^2 \rangle \tag{5}$$

Table 2 shows the average asymmetries over both the electron and photon detector faces and associated times needed to reach a 1% precision level. To calculate the time needed for a single bunch measurement in the table we conservatively used $\langle A \rangle^2$, which can be improved depending on the spatial resolution of the detector. For these calculation a 532 nm wavelength laser with a polarization of 100% and a beam polarization of 85% was used. Additionally assuming one interaction per crossing for each bunch one can calculated the needed luminosity from the laser bunch interaction.

beam energy [GeV]	σ_{unpol} [barn]	$\langle A_\gamma \rangle$	t_γ[s]	$\langle A_e \rangle$	t_e[s]	L[1/(barn·s)]
5	0.569	0.031	184	0.029	210	1.37E+05
12	0.482	0.057	54	0.056	56	1.62E+05
18	0.432	0.072	34	0.075	31	1.81E+05

Table 2: Asymmetries, measurement times needed for a 1% statistical measurement for one bunch and needed luminosities for three different beam energies for a 532 nm laser.

The information on the last column of table 2 can give some constraints on the power needed in the laser system. Following the derivation in [8] we can determine the luminosity of two beams with a crossing angle α:

$$\mathcal{L} = f_0 N_1 N_2 \frac{\cos(\alpha/2)}{2\pi} \frac{1}{\sqrt{(\sigma_{x,1}^2 + \sigma_{x,2}^2)}} \frac{1}{\sqrt{(\sigma_{y,1}^2 + \sigma_{y,2}^2)\cos^2(\alpha/2) + (\sigma_{z,1}^2 + \sigma_{z,2}^2)\sin^2(\alpha/2)}} \tag{6}$$

Using the electron beam parameters from table 1 as well a 10W 532 nm laser system pulsed at the 18 GeV bunch frequency with a transverse width of 100 μm for both the vertical and horizontal direction gives a luminosity of about $6 \cdot 10^5$ 1/(barn·s). This is a factor of 4 larger than the needed luminosity extacted from table 2. Calculations with the beam parameters for 10 and 5 GeV result in a luminosity of $5 \cdot 10^5$ 1/(barn·s), still sufficient for a differential measurement. Figure 8 shows the luminosity for this configuration as a function of crossing angle between the electron and laser beams.

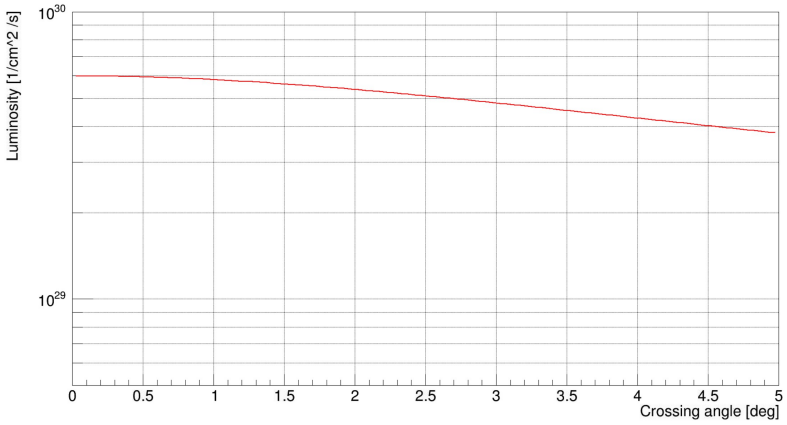

Figure 8: Luminosity as a function of crossing angle for a 10W 25MHz laser.

As can be see from figure 15 the extent of the scattered particles at the detector plane is quite limited. For the photon detector the extent is approximately 12, 6, 4 mm in both x and y (for 5, 10, and 18 GeV respectively), while for the electron detector the scattered particles span approximately 6, 12, 16 cm in x (for 5, 10, and 18 GeV respectively) and slightly more than 400 μm in y. A preliminary analysis was performed where the asymmetry was extracted from simulated data set. Different detector pitch showed that systematic effects appear with detector segmentation larger than 200 μm for the photon detector. For the electron detector the extraction of the asymmetry deviated from the injected asymmetry once detector segmentation was larger than 50 μm. Furthermore, the detectors need to be able to be able to detect one scattered particle for each bunch with a top rate of 99MHz (see table 1 for details).

Selection of an adequate detector technology for either the photon or electron detectors is predicated on a full analysis of the background environment at the polarimeters. However, due to the stringent spacial constraints, the fast response time needed, and potential high radiation environment a technology like the diamond strip detector previously tested by Alexandre Camsonne (reported in the first YR meeting [4]) could meet these requirements. This test showed that an electronics chain can be made that will result in a full pulse width smaller tha 10ns (the

distance between consecutive bunches at 5 and 10 GeV). Other technologies such as those envisioned for the Roman Pots, or HVMAPs will be evaluated as the project proceeds.

2 Laser system requirements

As described in the previous section, a single pass, pulsed laser is sufficient to make a precise measurement (dP/P $\approx$ 1%) of the polarization of each bunch. While a wavelength of 1064 nm appears to be adequate (see table 3), there are certain advantages to using a smaller wavelength (532 nm). The larger analyzing power results in shorter measurement times, while the backscattered photons (and scattered electrons) will be emitted in a larger cone, putting less stringent requirements on the detector segmentation.

beam energy [GeV]	σ_{unpol} [barn]	$\langle A_\gamma \rangle$	t_γ[s]	$\langle A_e \rangle$	t_e[s]	L[1/(barn·s)]
5	0.339	0.017	613	0.015	787	2.31E+05
12	0.327	0.034	158	0.033	161	2.39E+05
18	0.333	0.046	84	0.046	84	2.35E+05

Table 3: Asymmetries, measurement times needed for a 1% statistical measurement for one bunch and needed luminosities for three different beam energies for a 1064 nm laser.

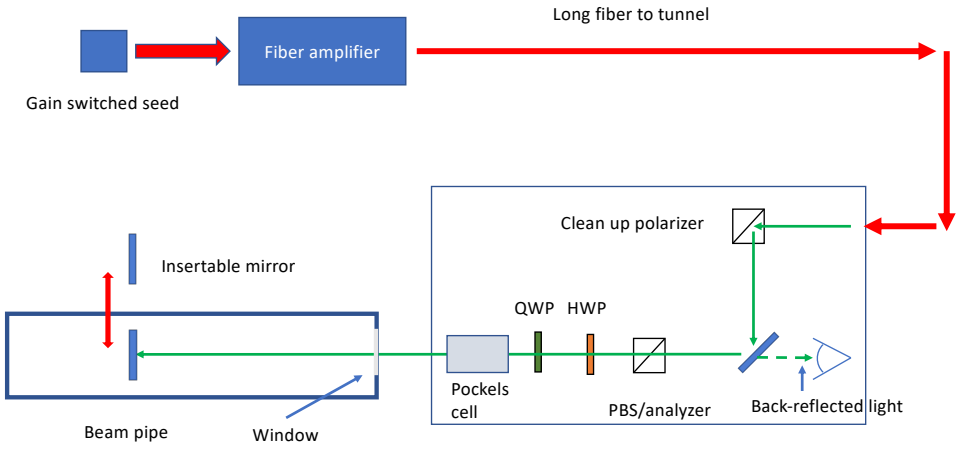

Figure 9: Suggested schematic layout for the EIC Compton laser system.

Figure 9 shows a sketch of the proposed laser system. The ideal laser system would have the following properties:

1. Average power up to 10 W. This power is only required at the highest beam energy (18 GeV), and even then is probably about a factor of 2 more than strictly required. However, transport of the laser to the interaction point will result in power loss, and a factor of two should provide sufficient margin.

2. Variable repetition rate. The ideal laser system would be able to match the repetition rate of the electron beam, $\approx$ 100 MHz at 5 and 10 GeV and $\approx$ 25 MHz at 18 GeV. In addition, it would also be useful to have the flexibility to decrease the laser frequency in the event that the Compton detector response times are longer than the 10 ns bunch spacing at 5 and 10 GeV. For example, a 10 MHz repetition rate would allow a 100 ns space between consecutive laser-electron beam collisions. Finally, it could be useful to make measurements of one and only one bunch on the ring at a time - in this case a repetition rate of 78 kHZ is required. The energy per bunch at each frequency will remain the same.

3. The laser should be close to diffraction limited to allow the beam size at the interaction point to be somewhat smaller than the electron beam size. This will allow measurements of the polarization profile across the beam.

4. The laser pulse width should be smaller than the 30-60 ps puslewidth (RMS) of the electron beam. This will allow measurement of the polarization across the longitudinal profile of the electron beam bunch.

5. The laser system should also include the ability to precisely control the laser polarization at the interaction point and flip the laser helicity rapidly - this latter requirement can be accomplished with a fast pockels cell.

The above requirements are most easily accomplished using a gain-switched seed laser, amplified by a fiber amplifier. Such systems are available at 1064 nm - if a green laser beam is desired, a frequency doubling crystal (either PPLN or LBO) will be required as have been routinely put in operation at Jefferson Lab (LERF).

The gain switched seed laser consists of a low power diode laser, biased with a DC voltage close to lasing threshold (the design is based on [5] and can be seen in figure 10). The application of an additional RF voltage results in pulsed output at the frequency of the applied RF. Pulse widths can vary with diode laser, but widths on the order of a few to 10s of ps are typical. In our case, the output of the gain switched seed requires pre-amplification before being sent to a high power fiber amplifier. Both the pre-amplifier and high power amplifier are commercially available products with several viable vendors. The gain switched system proposed here is modelled on the laser system that has been in use for several years at the JLab polarized electron source. The main differences are related to the wavelength (1064 nm for the seed) and the overall power desired. The latter requirement is achieved simply by obtaining a higher power fiber amplifier for the final stage.

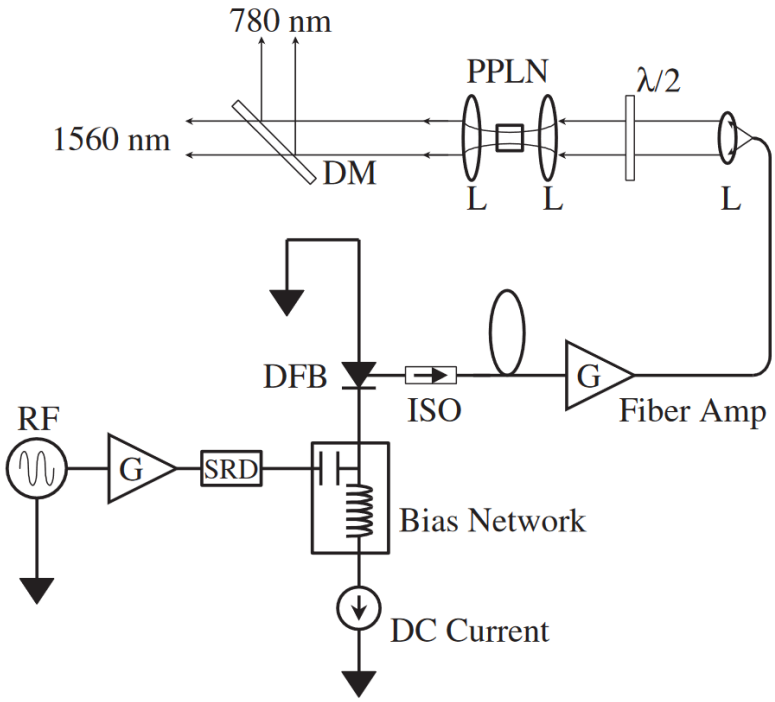

Figure 10: Schematic of the CEBAF injector fiber-based laser system. (Figure 1 of [5] DFB is a distributed feedback Bragg reflector diode laser; ISO is a fiber isolator; SRD is step recovery diode; L is a lens; PPLN is a periodically-poled lithium niobate frequency-doubling crystal; DM is a dichroic mirror.)

In addition to the laser system itself, it is crucial to be able to reliably determine the degree of circular polarization of the laser in the beamline vacuum. While it is relatively straightforward to measure laser polarization, such measurements in vacuum can be challenging. It is not sufficient to measure the laser polarization outside the vacuum system and assume that it is the same in the beam pipe - birefringence in the vacuum window can change the laser polarization, and even worse, the birefringence changes under mechanical stress, i.e., when flanges are tightened and under vacuum stress.

Fortunately, the laser polarization inside the beamline can be constrained using an optical reversibility theorem. This is illustrated in Fig. 11. Linearly polarized light (ϵ_1) is transformed to a general elliptical state (ϵ_2) via polarization modifiying optics, which may include wave plates and other birefrignent elements (including the vacuum window), and is represented by a matrix M_E. Upon reflection, the light with polarization (ϵ_3) passes through the same birefringent elements in reverse order (represented by $(M_E)^T$). The optical reversibility therorem states that for initial linear polarization (ϵ_1), the final resulting polarization (ϵ_4) is linear and orthogonal to the initial polarization, if and only if the polarization just before the mirror (ϵ_2) is 100% circular [7]. This scheme was successfully employed in experimental Hall C at Jefferson Lab, where the DOCP of the laser was set to 100% with an uncertainty better than 0.2%. In the Hall C setup (which would be replicated here), the DOCP was maximized

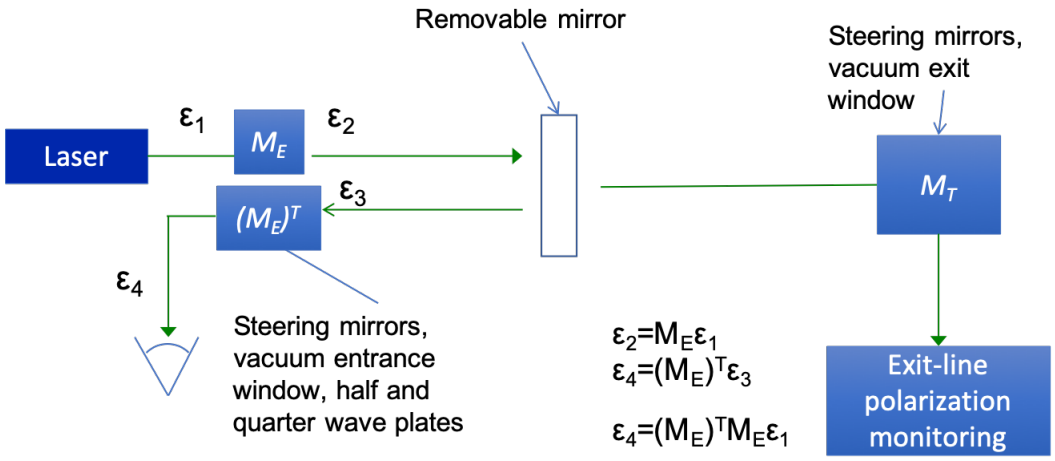

Figure 11: Illustration of the optical reversibility theorem and its application for monitoring the polarization of the Compton laser inside the beamline vacuum.

by simply minimizing the amount of back-reflected light transmitted through an anlyzer (see Fig. 12). In application for the EIC Compton, a removable mirror would be inserted to setup the laser polarization at the interaction point. A polarization monitoring system in the laser exit line (after the laser exits the vacuum enclosure through a window) would then be used to non-invasively monitor the time dependence of the polarization.

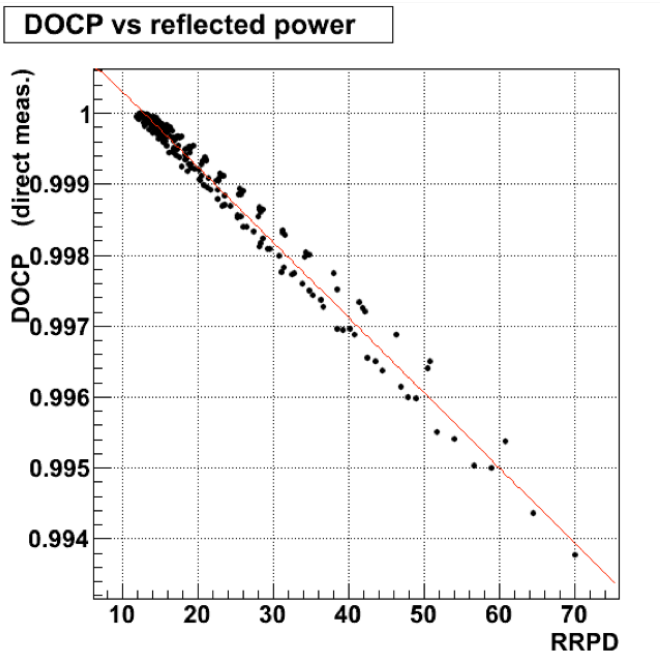

Figure 12: Calculated DOCP vs. reflected power for measurements from the Hall C Compton polarimeter.

3 Proposed work plan and budget

The activities in this proposal will consist of two main parts:

1. Construction and characterization of a prototype laser system for the EIC Compton polarimeter. This will entail fabrication of the gain switched seed laser system and its subsequent amplification in a fiber amplifier at 1064 nm. The resulting laser pulse-width, linewidth, and beam shape (M^2) will be characterized. As part of this exercise, we will also build a fiber delivery system to allow the high power laser to be transported up

to 20 m away. We will check that the laser output characteristics are unaffected after this tranport. This exercise is important to make sure that we can place the seed laser and fiber amplifier a reasonable distance from the EIC electron beam and reduce risk of component damage due to radiation.

Upon achieving the desired properties at 1064 nm, we will frequency double the 10 W fiber amplifier output to 532 nm using an LBO doubling system. The frequency doubled light will be characterized as above.

2. Development of a system for setting the laser polarization to 100% DOCP inside the beamline vacuum. This work will require two remotely controlled rotation stages for controlling the initial polarization state, and a third rotation stage for directly measuring the polarization (using the rotating quarter-wave plate technique, or similar) before the region is placed under vacuum. For this step, we will place a fixed mirror in a vacuum chamber - a movable mirror will be required for the final system, but this is not necessarily required at this stage.

Item	Cost[$]
Seed: Laser diode	12000
Seed: Pulse driver	20000
Seed: Preamplifier	10000
Seed: Controllers	13000
Seed: Fiber optics	5000
Gain switched seed and preamplifier total	**60000**
Fiber power amplifier	45000
Single-mode fiber (20m)	5000
Frequency doubler	5000
Total	115000

Table 4: Basic list of items needed to build the proposed laser system.

We envision a 3-year timeline for the project to achieve the steps above.

1. Year 1: Initial design of the laser system, purchasing of components and start laser construction
2. Year 2: Finalize construction, and characterization of laser system on laser table. Prove multi frequency operation. Design vacuum system.
3. Year 3: Confirm DOCP measurement through vacuum window and publish results

For the laser itself table 4 shows the expected cost based on prices currently available from different vendors. Note that, this particular fiber-amp is 10W IR and depending on the final design may need to be upgraded to provide sufficient power (if 532 nm is the needed configuration). Additional equipment needed for the characterization of the laser (such as CCD camera or an auto-correlator to measure pulse width) will be borrowed from other laser labs at Stony Brook University or Jefferson Lab. For the Year 3 vacuum window test an estimate for the vacuum chamber will be available following the completion of the design (end of Year 1).

The laser table components and their cost needed to prepare the laser state and control the DOCP are listed in table 5.

Item	Cost[$]
QWP (2)	1000
HWP	500
Pockels cell	2500
Polarizing cubes (3)	260
Mirrors (10)	700
Remote controlled stages (3)	10700
Picomotor controller (2)	3100
Assorted stands	2000
Total	20760

Table 5: Basic list of items needed to set constrain the degree of circular polarization at the collision point via the back-reflection technique.

The costs listed in tables 4 and 5 are components needed exclusively for the EIC Compton and make up the bulk of the cost for the R&D project. They are estimated by referencing the Thorlabs online catalogue and through communications with a fiber amplifier vendor (for the fiber power amplifier). We will pursue other funding stream to partially fund the project and complement contributions from the EIC R&D (such as the Stony Brook University OVPR fund).

A Document changes since preproposal

- Included preliminary detector requirements: count rate, segmentation and timing.
- Expanded description of the gain switched laser and added justification for expenditures.
- Included Pockels cell in the design (and cost) to allow for fast flipping of the laser polarization to aid in systematic studies.
- Added appendix with large scale figures.

B Large Scale Figures

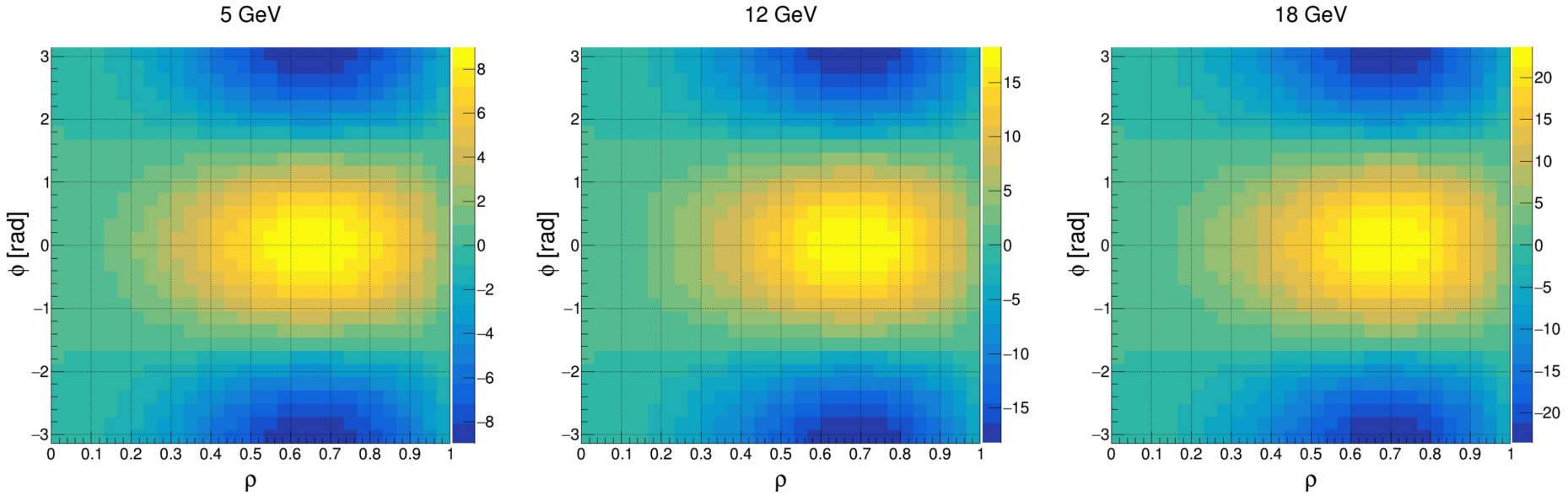

Figure 13: Compton transverse asymmetry (z-axis) as a function of back-scattered photon energy and azimuthal scattering angle.

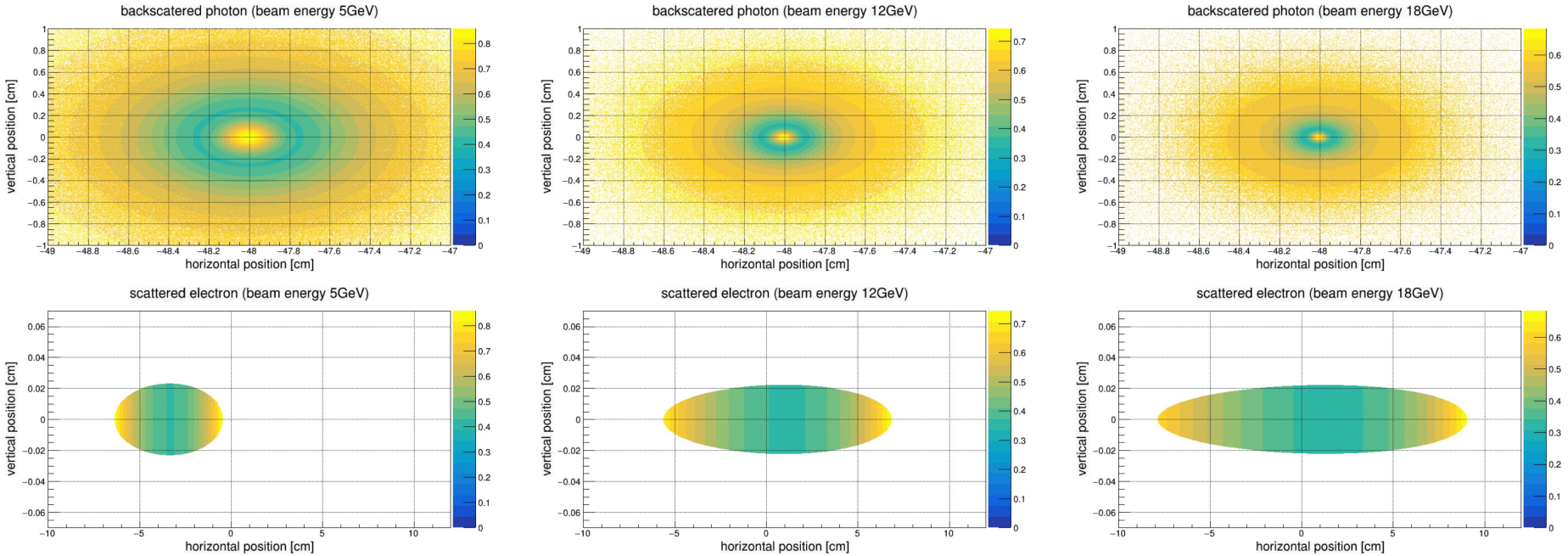

Figure 14: Compton unpolarized cross-sections (on the z axis) as a function of transverse position for 3 different beam energies.

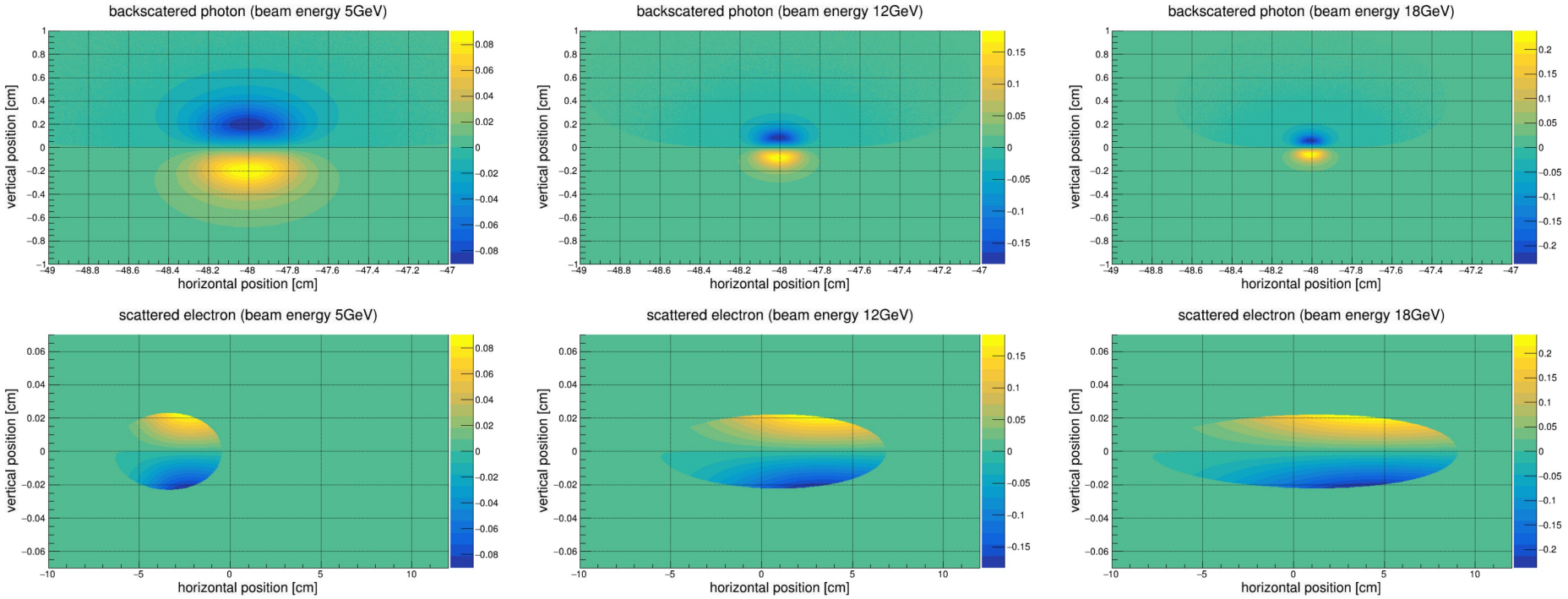

Figure 15: Compton analyzing powers (on the z axis) as a function of transverse position for 3 different beam energies.

References

[1] D. Androic et al. Precision measurement of the weak charge of the proton. *Nature*, 557(7704):207–211, 2018.

[2] Kurt Aulenbacher, Eugene Chudakov, David Gaskell, Joseph Grames, and Kent D. Paschke. Precision electron beam polarimetry for next generation nuclear physics experiments. *Int. J. Mod. Phys.*, E27(07):1830004, 2018.

[3] G. Bardin et al. Conceptual design report of a compton polarimeter in cebaf hall a. *JLab Internal note*, 1996.

[4] Alexandre Camsonne. Compton polarimetry for EIC, 2020. Slide 19, Accessed: 2020-07-01.

[5] J. Hansknecht and M. Poelker. Synchronous photoinjection using a frequency-doubled gain-switched fiber-coupled seed laser and eryb-doped fiber amplifier. *Phys. Rev. ST Accel. Beams*, 9:063501, Jun 2006.

[6] Blanka Sobloher, Riccardo Fabbri, Ties Behnke, Jan Olsson, Daniel Pitzl, Stefan Schmitt, and Justyna Tomaszewska. Polarisation at HERA - Reanalysis of the HERA II Polarimeter Data -. *HERA Internal Note*, 1 2012.

[7] N. Vansteenkiste, P. Vignolo, and A. Aspect. Optical reversibility theorems for polarization: application to remote control of polarization. *J. Opt. Soc. Am. A*, 10(10):2240–2245, Oct 1993.

[8] S. Verdú-Andrés. Luminosity geometric reduction factor from colliding bunches with different lengths. *BNL CA-D Internal Note*, 2017.